metals

MDPI

Article

Optimization of V-Bending of Grade 4 Titanium Bone Plates: A Combined Experimental, Numerical, and Artificial Intelligence Approach

Hamza Guelbi [1], Sami Chatti [1,2], Borhen Louhichi [3,*] and Mohamed Ali Terres [1,4]

[1] Sousse Higher Institute of Applied Sciences and Technology (ISSATSo), University of Sousse Cité Taffala, Ibn Khaldoun, Sousse 4003, Tunisia; hamzaguelbi@gmail.com (H.G.); s.chatti.issat@gmail.com (S.C.); mohamedali.terres@esstt.rnu.tn (M.A.T.)
[2] Laboratory of Mechanics of Sousse, National School of Engineers of Sousse, (ENISo), University of Sousse, Route de Ceinture Sahloul, Cité Hammam Maarouf, Sousse 4054, Tunisia
[3] Deanship of Scientific Research, Imam Mohammad Ibn Saud Islamic University (IMSIU), Riyadh 11432, Saudi Arabia
[4] Laboratory of Mechanics, Materials and Processes (LMMP), National High School of Engineering of Tunis (ENSIT), University of Tunis, 5 Avenue Taha Hussein, Montfleury, Tunis 1008, Tunisia
* Correspondence: blouhichi@imamu.edu.sa

Abstract

The cold V-bending of Grade 4 titanium bone plates at room temperature is a critical forming operation that must be optimized to control strain localization and springback and to reduce the risk of surface cracking. This study proposes a combined experimental, numerical, and artificial intelligence-based approach for the analysis and optimization of this process. Tensile tests were first performed to characterize the mechanical behavior of the material and to calibrate the constitutive law used in the finite element model. The numerical model was then validated through comparison with experimental V-die bending results. A design of experiments was subsequently applied to investigate the effects of sheet thickness, die shoulder distance, punch radius, and punch displacement on two key responses: equivalent plastic strain (PEEQ) and spring back. The results show that sheet thickness and die shoulder distance are the most influential parameters. In addition, artificial neural network models were developed to predict process responses, and Bayesian regularization showed the best overall predictive performance among the tested ANN training algorithms, namely Levenberg–Marquardt, Bayesian regularization, and scaled conjugate gradient. The proposed framework provides a basis for optimizing the forming of titanium orthopedic implants.

Keywords: Grade 4 titanium; orthopedic implants; V-bending; sheet metal forming; spring back; equivalent plastic strain; process optimization

Check for updates

Academic Editor: Yanxin Qiao

Received: 4 June 2026
Revised: 15 June 2026
Accepted: 20 June 2026
Published: 29 June 2026

Copyright: © 2026 by the authors. Licensee MDPI, Basel, Switzerland. This article is an open access article distributed under the terms and conditions of the Creative Commons Attribution (CC BY) license.

1. Introduction

Bending is a fundamental forming operation widely used in the automotive, aerospace, and biomedical sectors. In orthopedic applications, the bending of titanium plates is particularly important because the final geometry, strain distribution, and spring back directly affect implant fit and structural integrity. However, controlling spring back, strain hardening, and fracture during the forming of titanium sheets remains challenging, especially when thin sections and severe bending conditions are involved. Previous studies have investigated the effects of process parameters [1–4], advanced numerical modelling

strategies [5–9], and artificial intelligence (AI) techniques [10–13] to improve the prediction and optimization of bending behavior. These developments are especially relevant to the manufacturing of reliable biocompatible medical devices, where dimensional accuracy and material integrity are critical.

Among metallic biomaterials used in orthopedic applications, commercially pure titanium and titanium alloys are widely employed because of their favorable combination of strength, corrosion resistance, and biocompatibility [14]. From a forming point of view, titanium sheets are known to exhibit limited room-temperature formability and pronounced spring back, which makes process control particularly important in bending applications [15]. In addition, the bending response of rolled titanium sheets may be strongly affected by anisotropy induced by rolling texture, which can influence yield behavior, strain localization, and spring back [16].

Conventional approaches based solely on force-drop measurements are often insufficient for accurately characterizing bending-induced damage, particularly in ductile metallic sheets [1]. For this reason, alternative strategies have been developed, including bending moment analysis, thickness evolution monitoring using digital image correlation (DIC), and strain-based characterization methods [1,5,9]. Process optimization in bending depends on several variables, such as temperature, punch speed, holding time, tool geometry, and sheet thickness [2,3,17]. Among the resulting phenomena, spring back remains one of the main challenges in sheet metal forming [7,18–21], especially in biomedical applications, where the final implant shape must closely match patient-specific anatomical requirements.

Because bending behavior depends on both material response and process conditions, an interdisciplinary approach is required. The finite element method (FEM) has become an essential tool for analyzing bending operations and is often combined with optimization techniques such as the Taguchi method [4] and genetic algorithms [2,8]. Improved predictive accuracy also depends on an appropriate description of material behavior, including strain hardening, anisotropy, and tension–compression asymmetry [2,5,22]. These aspects are particularly important in the design of biomedical components, which must satisfy both biocompatibility requirements and mechanical reliability under service loading.

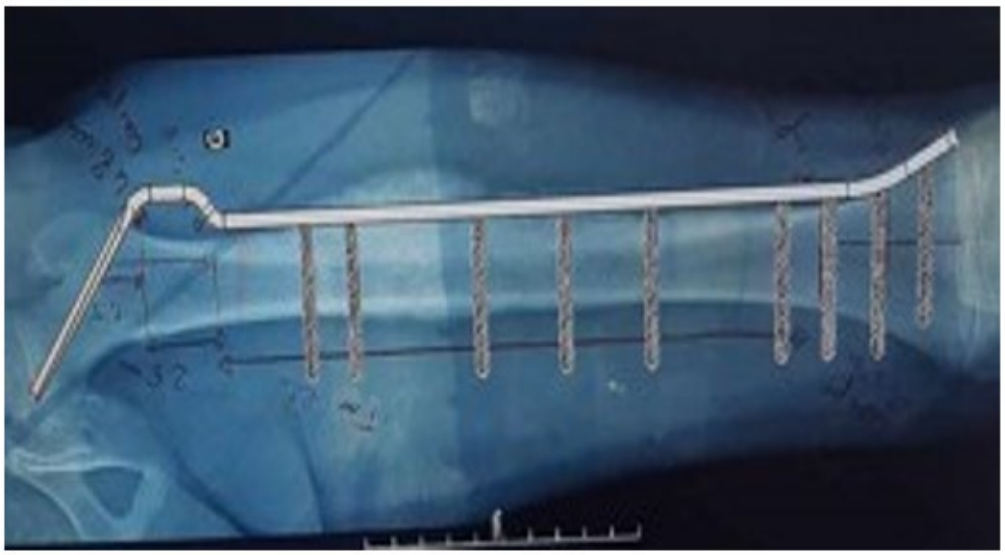
More recently, machine learning (ML) methods, particularly artificial neural networks (ANNs), have been used to predict spring back and assist in process optimization [9–11,13]. Such approaches are promising for the development of efficient and reliable manufacturing routes for customized implants. In this context, the present study combines experimental characterization, finite element modelling, and ANN-based prediction to analyze the V-bending behavior of Grade 4 titanium bone plates. The specific objectives are to identify the most influential process parameters, to predict equivalent plastic strain and spring back, and to provide a framework for process optimization.

2. Material and Methods

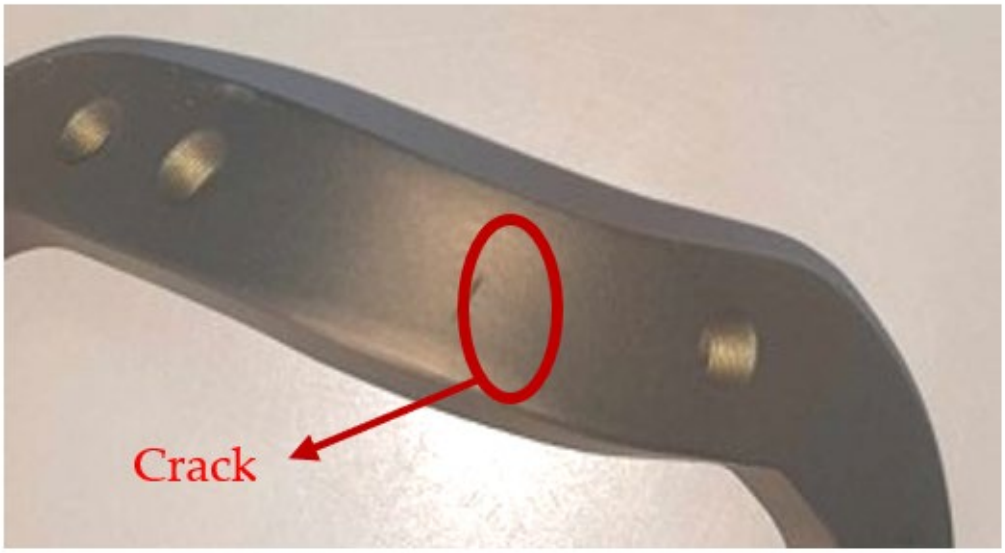
2.1. Material

The cold bending of Grade 4 titanium bone plates, as demonstrated in Figure 1, is a critical step in the manufacturing of orthopedic implants. In this study, particular attention is paid to the effects of process parameters on deformation severity and spring back, as excessive strain localization during forming may increase the risk of surface cracking. Understanding these effects is essential for improving the reliability and mechanical integrity of bent plates intended for biomedical use. Titanium and its alloys are widely used for orthopedic implants because of their high specific strength, low density [3], excellent corrosion resistance, and good biocompatibility. Furthermore, the biocompatibility of titanium

has been proven to reduce the risk of rejection or adverse reactions, making it an ideal choice for orthopedic applications. The chemical composition and the main mechanical properties of the material are summarized in Tables 1 and 2, respectively.



(a)



(b)

Figure 1. Grade 4 titanium bone plate: (**a**) example of a bone plate used in orthopedic fixation, and (**b**) crack observed after bending.

Table 1. Chemical compositions of the grade-4 CP-Ti (wt.%).

Material	O	N	H	Fe	C	Ti
CP-Ti Grade-4	0.30	0.009	0.0028	0.206	0.012	Bal.

Table 2. Mechanical properties of commercially pure titanium.

Material	E (GPa)	Re (MPa)	Rm (MPa)	A (%)	Alloy Type
CP-Ti Grade-4	104	483	550	15	α

The methodology includes three main steps. First, tensile tests were performed to identify the mechanical behavior of Grade 4 titanium. Second, a finite element model implemented in Abaqus ((R2026x) was calibrated and validated using bending experiments. Third, the validated model was used to simulate the V-die bending process and to generate the dataset required for statistical analysis and ANN-based prediction.

2.2. Tensile Test

The mechanical properties of the material were determined by quasi-static tensile tests performed at room temperature. This testing was conducted using a 200 kN MTS machine (MTS, USA, Sousse, Tunisia), in accordance with the standards set out in ASTM E8/E8M [23]. The specimens were machined by CNC milling at a feed rate of 1500 mm/min, according to the geometry shown in Figure 2 and the dimensions listed in Table 3.

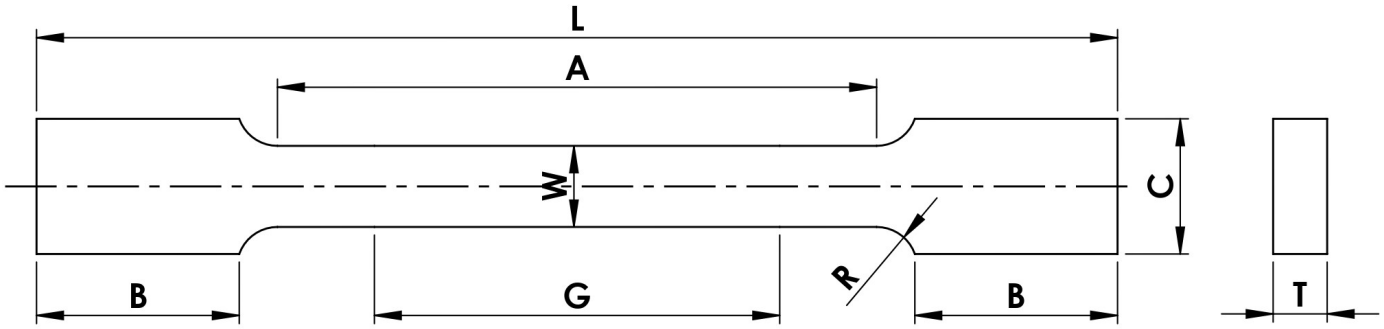


Figure 2. Tensile specimen geometry.

Table 3. Dimensions of sub-size Specimen.

Dimension	mm
G-Gauge length	25.0 ± 0.1
W-Width	6.0 ± 0.1
T-Thickness	5
R-Radius of fillet, min	6
L-Overall length, min	100
A-Length of reduced section, min	32
B-Length of grip section, min	30
C-Width of grip section, approximate	10

This machining procedure reduces edge damage that may arise from thermally induced cutting effects. To ensure repeatability, at least three specimens were tested for each condition after preliminary measurements of thickness and width. In addition, tensile tests were carried out along different rolling directions in order to assess the possible anisotropy of the material (Figure 3). The specimen orientations were defined with respect to the rolling direction according to the conventional 0°, 45°, and 90° configuration reported in [24].

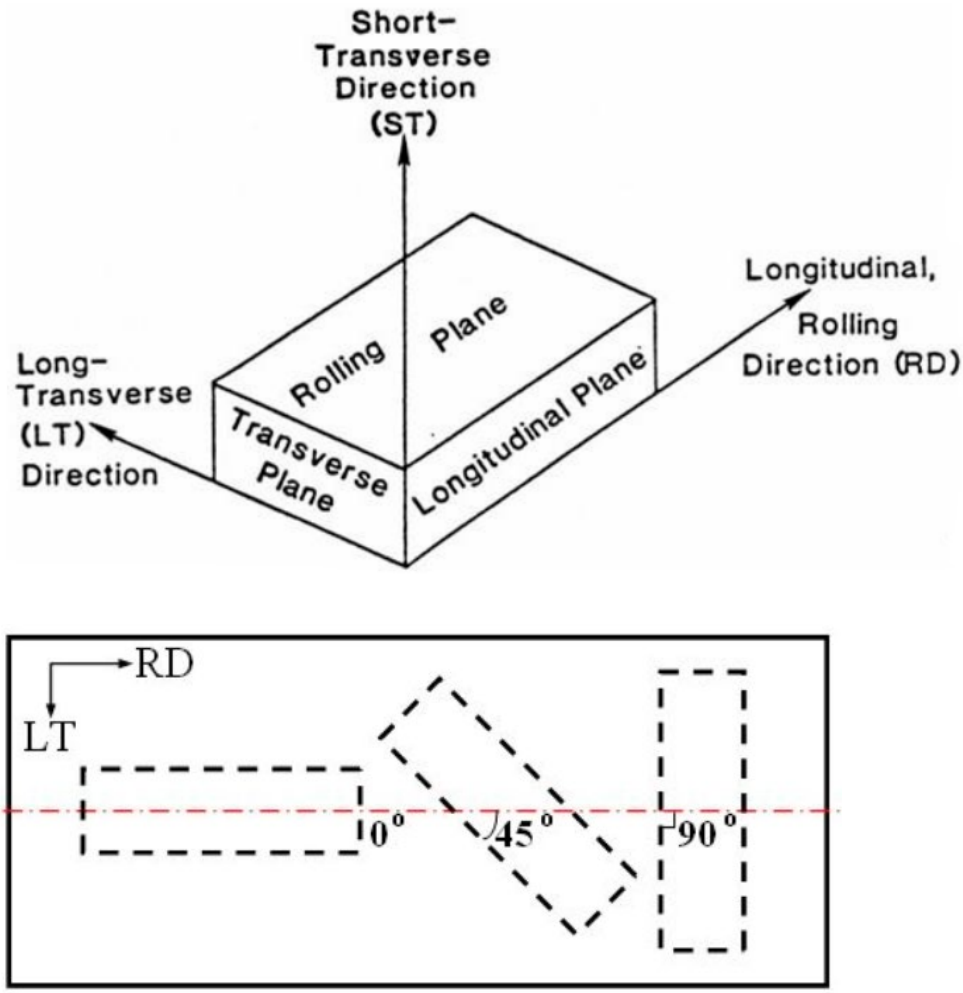


Figure 3. Orientation of tensile specimens relative to the rolling direction of the sheet: 0°, 45°, and 90°. Adapted from ref. [24].

Digital image correlation (DIC) was used as a non-contact technique for strain measurement. The specimen surface was first coated with a commercially available matte white spray paint for metal surfaces in order to obtain a uniform, non-reflective background, and was then covered with a random black speckle pattern before being mounted in the testing machine MTS, Sousse, Tunisia (Figure 4a). The region of interest (ROI) was illuminated using a 20 W LED source, and images were captured with an Impirex ICL-B16 camera ((Imperx, Inc., Boca Raton, FL, USA)) (Figure 4b). The recorded images were stored using EPIXXCAP STD V3.8 software and processed with GOM Correlate software 2026 to obtain the displacement and strain fields.

The starting material was a commercially supplied rolled Grade 4 titanium plate, from which tensile specimens were machined along the 0°, 45°, and 90° directions relative to the rolling direction. Although rolled titanium generally exhibits anisotropic behavior, the tensile curves obtained in the present study (Figure 5) showed only limited directional differences. These results therefore indicate low anisotropy in the investigated material rather than perfectly uniform properties. On this basis, an isotropic elastoplastic model was adopted as a first approximation for the V-die bending simulations. Nevertheless, the possible influence of anisotropy on local stress and strain distributions should not be neglected, and a more advanced anisotropic constitutive model may be considered in future work to improve predictive accuracy.

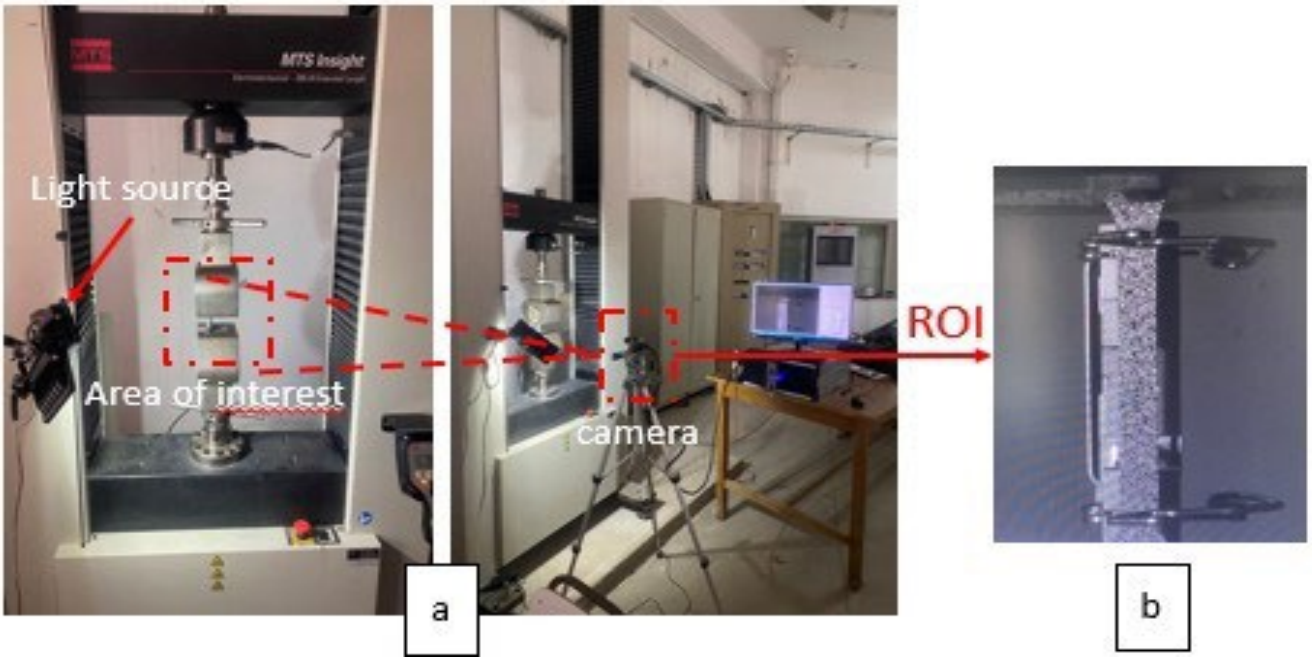


Figure 4. Tensile test: (**a**) tensile machine and (**b**) ROI for the DIC analysis.

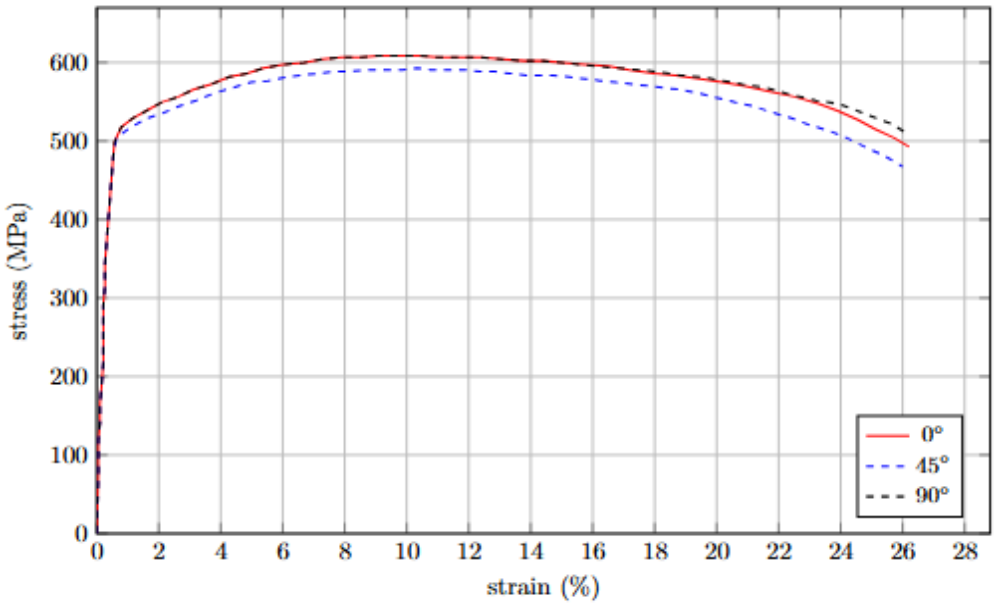


Figure 5. Stress-Strain Curves of Grade 4 titanium.

As illustrated in Figure 6, the DIC analysis was conducted during the tensile testing procedure, with the utilization of two extensometers. The resulting strain data (eps LX and eps LY) yielded an overall Poisson's ratio of 0.33.

The elastic behavior was described by Hooke's law, ($\sigma = E\varepsilon$), with a Young's modulus of E = 101 GPa. The plastic behavior was represented using the Swift hardening law, ($\sigma = K(\varepsilon_0 + \varepsilon)^n$). The identified material parameters are summarized in Table 4, and the corresponding fitted curve is shown in Figure 7. The yield stress was determined using the conventional 0.2% offset method.

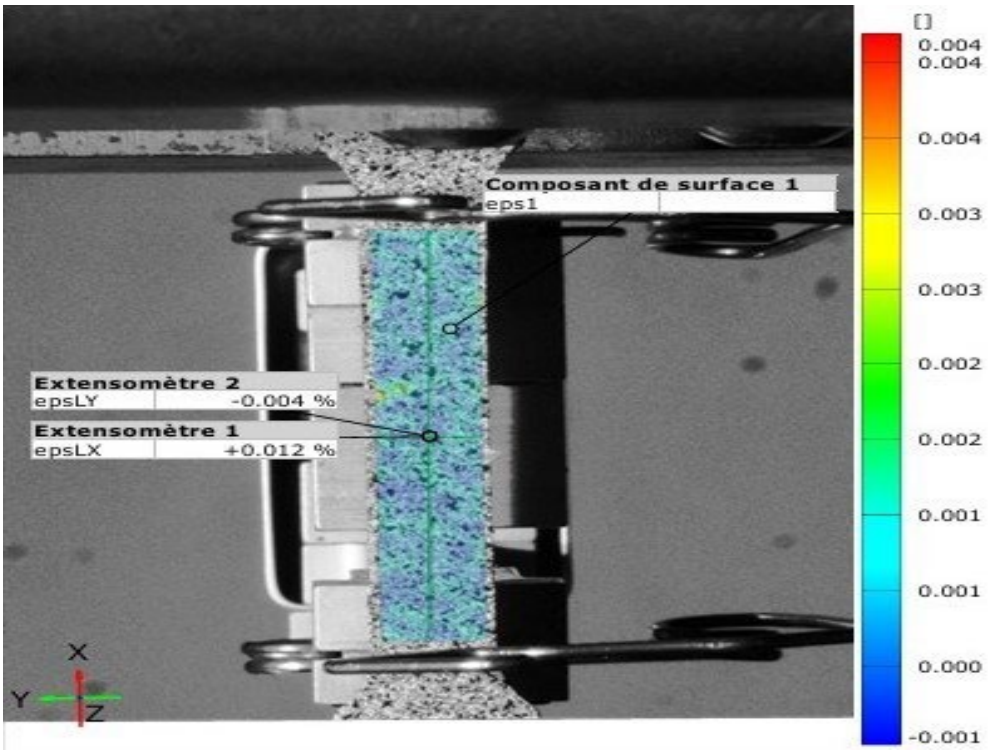


Figure 6. Determination of Poisson's Ratio via DIC and an extensometer.

Table 4. Swift law parameters.

Flow Stress Model	Expression	Material Parameters		
Swift hardening law	$\sigma = K\,(\varepsilon_0 + \varepsilon^p)^{\,n}$	K (MPa)	εo	n
		874.55	0.0104	0.12

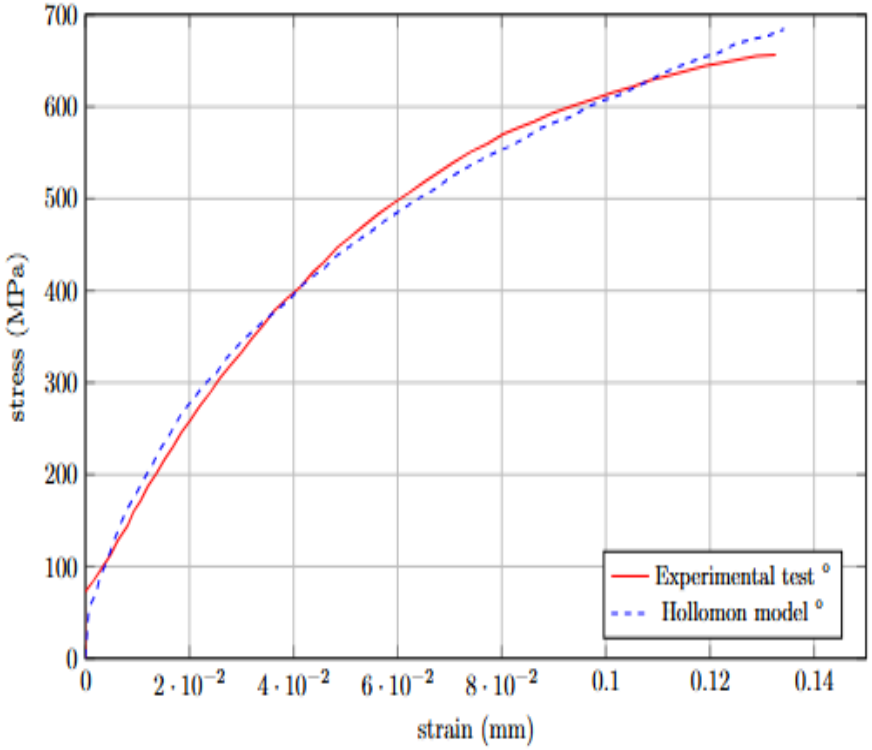


Figure 7. Material law and measurement for Grade 4 titanium.

2.3. V-Die Bending Process

V-bending tests (SOFEMED, Soliman, Tunisia) were carried out on rectangular Grade 4 titanium specimens with dimensions of 150 mm × 10 mm × 6 mm and a die shoulder distance of 100 mm. During the tests, the applied force and the corresponding displacement were continuously recorded until specimen failure. These experiments were primarily used to validate the material law and the numerical model under bending conditions. Minor irregularities observed near the maximum load may be related to local yielding or material heterogeneity and should be examined in future work.

2.4. Numerical Simulations of the Sheet Metal V-Die Bending Process

A finite element analysis was performed in Abaqus/Standard to validate the constitutive law identified from the tensile tests and to simulate the subsequent V-die bending process. A two-dimensional model of the Grade 4 titanium specimen was first developed to reproduce the V-die bending process and to capture the through-thickness deformation during bending (Figure 8). The material was described as an isotropic elastoplastic solid based on the tensile characterization results, while the numerical configuration reproduced the experimental V-die setup, including the die geometry, punch radius, die shoulder distance, and the imposed punch displacement.

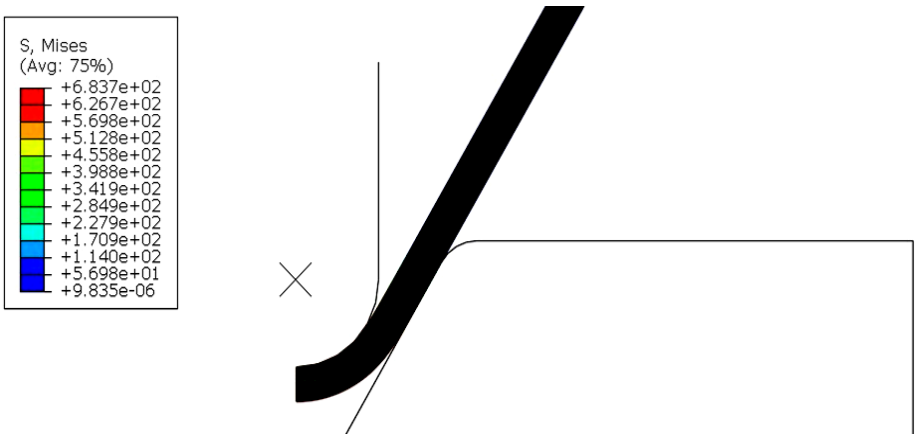


Figure 8. Finite element model of the V-die bending process.

In this model, the sheet was defined as a deformable body, whereas the punch and die were considered rigid tools. Geometrical symmetry was also exploited to reduce computational cost while maintaining satisfactory numerical accuracy.

A mesh convergence study was carried out to ensure the stability and reliability of the numerical solution. The mesh was generated using CPS4R elements, i.e., 4-node bilinear plane stress quadrilateral elements with reduced integration. The convergence study led to a mesh density of 120 elements along the width and 20 elements through the thickness. This discretization provided a satisfactory compromise between numerical accuracy and computational efficiency. The main outputs extracted from the simulations were equivalent plastic strain (PEEQ) and springback. PEEQ was used as an indicator of permanent deformation severity, whereas springback was used to assess dimensional accuracy after unloading.

The effects of die shoulder distance (L), punch radius (R), punch displacement (U), and sheet thickness (EP) on the V-bending response were investigated using a design of experiments (DOE) framework coupled with Abaqus simulations (Figure 9). These parameters were varied over several levels in order to quantify their influence on equivalent plastic strain and springback and to generate the dataset used for predictive modelling and process optimization.

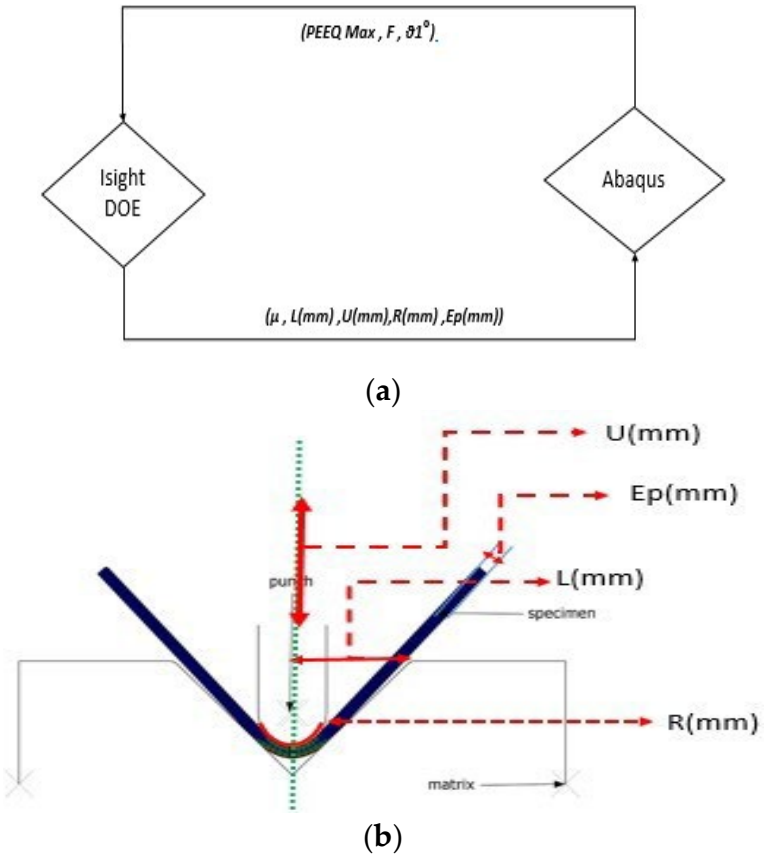


Figure 9. Design of Experiments: (**a**) (DOE) Methodology and (**b**) Parameter Definition.

3. Results

3.1. Validation of the Numerical Model

The numerical model was validated by comparing the simulated and experimental force-displacement curves obtained from the V-die bending tests. A good agreement was observed between the two responses (Figure 10), indicating that the adopted constitutive law and modelling assumptions provide a satisfactory description of the material behavior under bending conditions. This validation supports the use of the model for the subsequent V-die bending simulations.

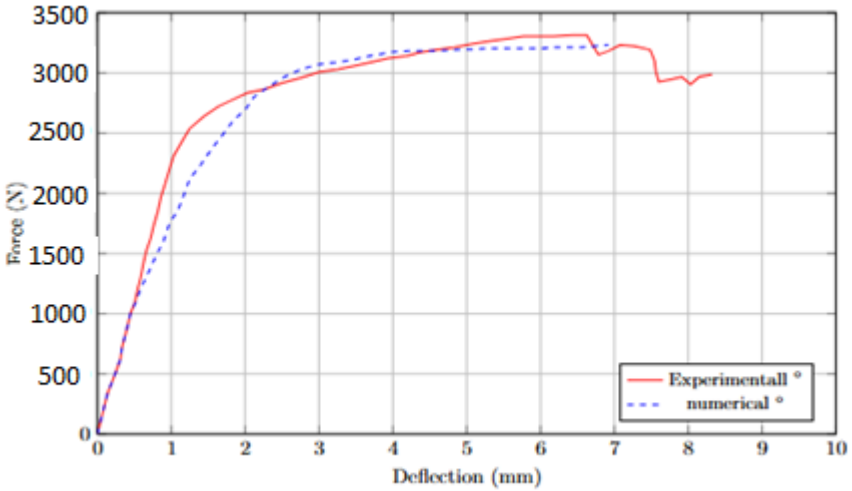


Figure 10. Comparison between numerical and experimental force-displacement curves for the V-die bending test.

3.2. Statistical Analysis

The design of experiments reported in Table 5 was used to analyze the effects of four input parameters on two main responses in the V-bending process: maximum equivalent plastic strain (PEEQ) and spring back. An analysis of variance (ANOVA) was then performed to identify the significant main effects and interactions and to support process optimization.

Table 5. Values and levels of bending parameters.

Parameters	Level 1	Level 2	Level 3	Level 4
EP (mm)	3	4	6	-
L (mm)	40	60	80	90
R (mm)	2	5	10	-
U (mm)	15	25	35	45

3.3. Influence of Process Parameters and Their Interactions on V-Bending Performance

The ANOVA results presented in Tables 6 and 7 indicate that the regression models for both equivalent plastic strain (PEEQ) and spring back are statistically significant ($p < 0.05$). Sheet thickness (A) and die shoulder distance (B) were identified as the most influential factors for both responses, with highly significant p-values ($p < 0.0001$). Punch radius (C) also affected both outputs, although its contribution was less pronounced, whereas punch displacement (D) significantly influenced PEEQ and had a weaker but still significant effect on spring back. Several interaction terms were also found to be significant, highlighting the importance of considering combined effects between the main process parameters, particularly sheet thickness, die shoulder distance, punch radius, and punch displacement, rather than only their isolated contributions. As shown by the perturbation plots in Figure 11, thickness had the strongest influence on spring back, which decreased as thickness increased, whereas die shoulder distance exerted the strongest effect on PEEQ. These trends are further supported by the predicted-versus-actual plots in Figure 12, which confirm the satisfactory predictive capability of the regression models despite some remaining discrepancies. The response surface analyses in Figures 13 and 14 provide additional insight into the effect of the process parameters: PEEQ varies moderately within the investigated parameter domain, with its main trends associated with thickness and die shoulder distance, while spring back is markedly more sensitive to thickness.

Table 6. ANOVA for density model for PEEQ.

Source	Sum of Squares	df	Mean Square	F-Value	p-Value
Model	2.02	10	0.1839	51.21	<0.0001
A-EP	0.4587	1	0.4587	127.77	<0.0001
B-L	0.9681	1	0.9681	269.64	<0.0001
C-R	0.0266	1	0.0266	7.41	0.0074
D-U	0.2368	1	0.2368	65.96	<0.0001
AB	0.1289	1	0.1289	35.89	<0.0001
AC	0.0724	1	0.0724	20.16	<0.0001
AD	0.0594	1	0.0594	16.55	<0.0001
BC	0.0603	1	0.0603	16.81	<0.0001
BD	0.0214	1	0.0214	5.95	0.0160
CD	0.0304	1	0.0304	8.46	0.0043

Table 7. ANOVA for density model for θ (°).

Source	Sum of Squares	df	Mean Square	F-Value	*p*-Value
Model	3099.61	8	387.45	60.95	<0.0001
A-EP	1783.75	1	1783.75	280.60	<0.0001
B-L	681.38	1	681.38	107.19	<0.0001
C-R	59.12	1	59.12	9.30	0.0028
D-U	38.11	1	38.11	5.99	0.0156
AB	146.87	1	146.87	23.10	<0.0001
AD	40.64	1	40.64	6.39	0.0126
A^2	260.35	1	260.35	40.96	<0.0001
B^2	34.40	1	34.40	5.41	0.0215

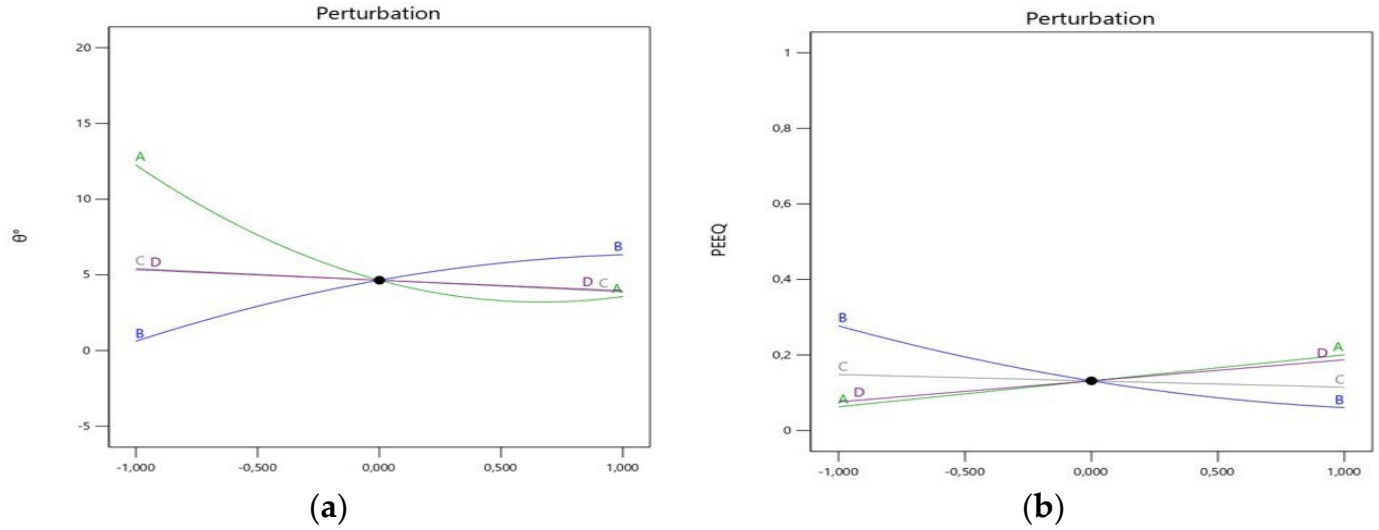


Figure 11. The perturbation plot: (**a**) θ° and (**b**) PEEQ.

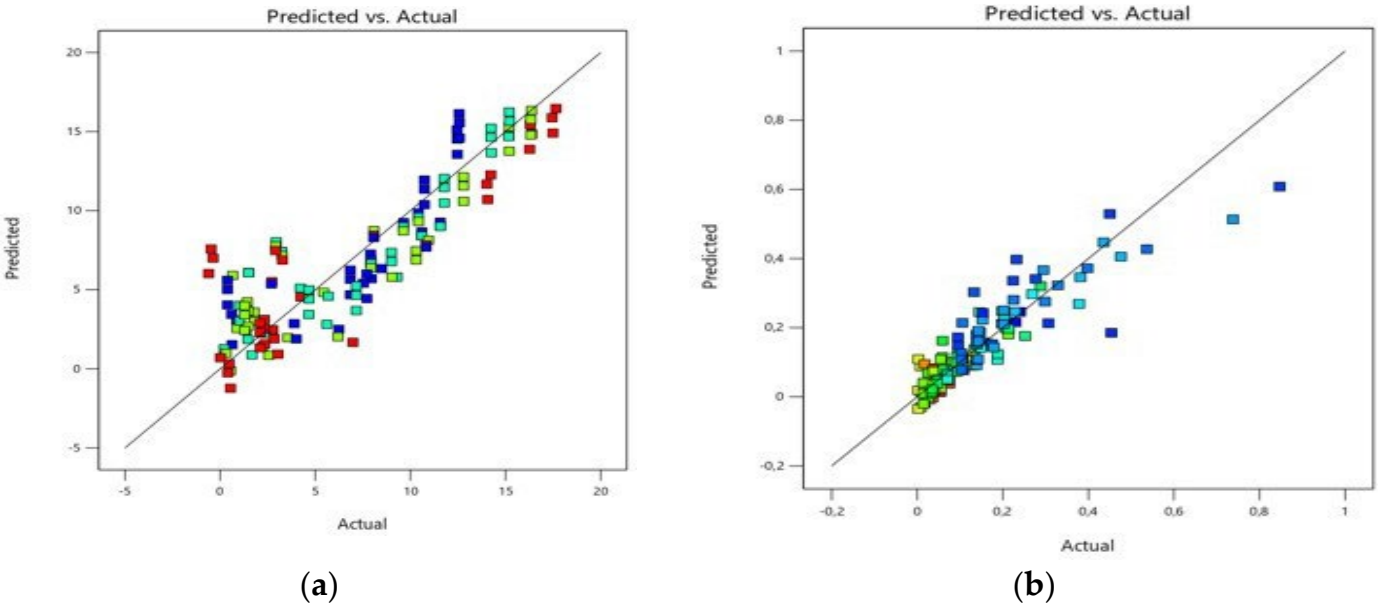


Figure 12. Prediction Accuracy Plot: (**a**) for θ° and (**b**) for PEEQ.

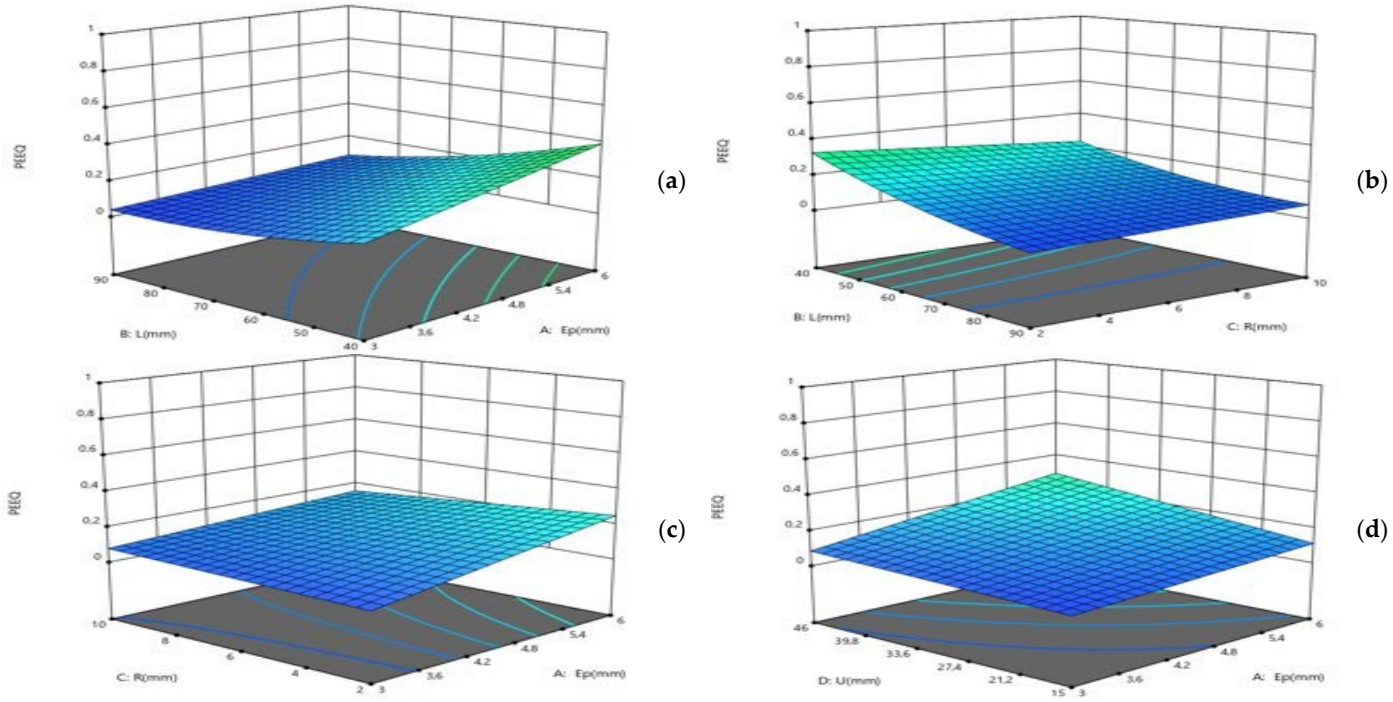


Figure 13. Response surface analyses for PEEQ combined effect: (**a**) EP and L; (**b**) EP and R; (**c**) EP and U; (**d**) L and R.

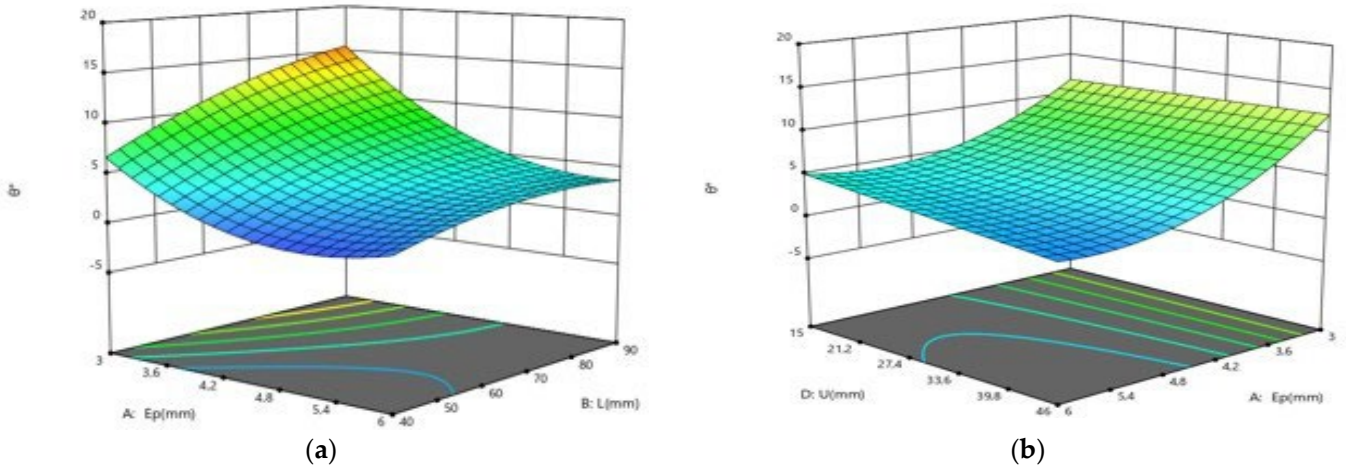


Figure 14. Response surface analyses for θ° Combined Effect. (**a**) EP and L; (**b**) EP and U.

In particular, increasing thickness leads to a clear reduction in spring back, whereas increasing die shoulder distance and punch displacement also tends to reduce the spring back angle, although to a lesser extent. The regression models therefore provide satisfactory predictions for both PEEQ and spring back, with R^2 values of 0.8102 and 0.7832, respectively (Table 8). The adjusted and predicted R^2 values remain acceptable, and the adequate precision values indicate a useful signal-to-noise ratio for both models. The remaining differences between predicted and observed values may be attributed to the simplified isotropic material description, the use of a single hardening law, and the presence of nonlinear interactions that are not fully captured by the current model. Further improvements could be achieved by incorporating anisotropic constitutive behavior, enlarging the dataset, and exploring more advanced optimization strategies.

Table 8. Model Performance Statistics.

Response	R^2	Adjusted R^2	Predicted R^2	Adeq Precision
PEEQ	0.8102	0.7943	0.7604	37.1801
θ (°)	0.7832	0.7703	0.7509	28.0524

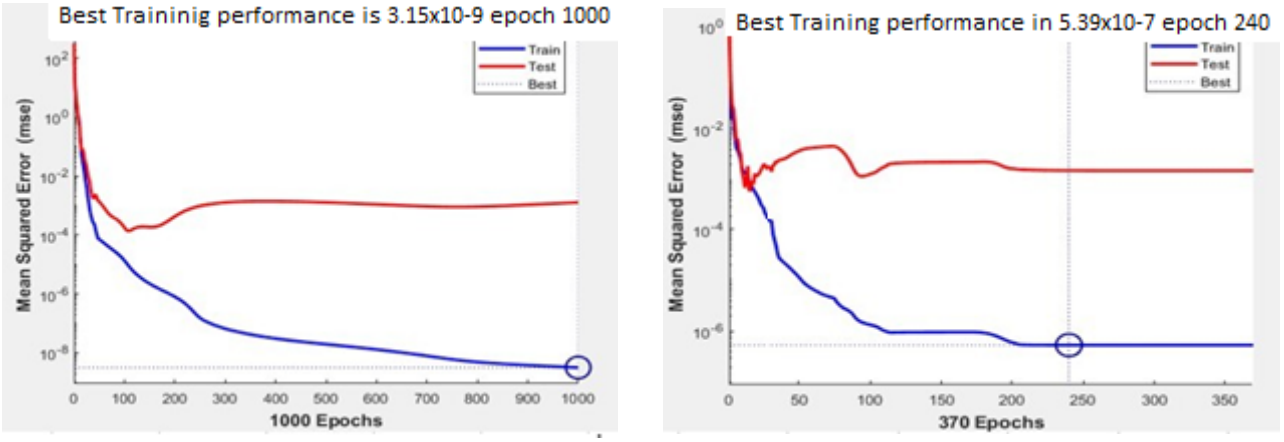
3.4. Artificial Neural Networks for Prediction

Three ANN training algorithms-Levenberg-Marquardt, Bayesian regularization, and scaled conjugate gradient, were evaluated for the prediction of spring back and PEEQ, as summarized in Table 9. The dataset was divided into training, validation, and testing subsets in proportions of 70%, 15%, and 15%, respectively. All networks were built with a single hidden layer containing 10 neurons.

Table 9. Algorithm Performance.

Algorithm	Output	R (Train)	R (Val)	R (Test)	MSE (Train)	MSE (Val)
Levenberg-Marquardt	θ°	1.000	0.996	0.995	3.8×10^{-5}	0.108
Bayesian regularization	θ°	1.000	0.997	1.000	3.2×10^{-9}	<0.001
Scaled conjugate gradient	θ°	0.960	0.890	0.936	2.18	0.104
Levenberg-Marquardt	PEEQ	0.969	0.862	0.823	1.3×10^{-5}	0.009
Bayesian regularization	PEEQ	1.000	0.973	0.978	5.4×10^{-7}	<0.001
Scaled conjugate gradient	PEEQ	0.949	0.955	0.958	1.5×10^{-3}	0.001

In the context of spring back prediction, both the Levenberg-Marquardt and Bayesian regularization algorithms demonstrated R-values that approached 1, thereby indicating the rapid convergence of the mean squared error (MSE), as reflected by the network performance curves shown in Figure 15.

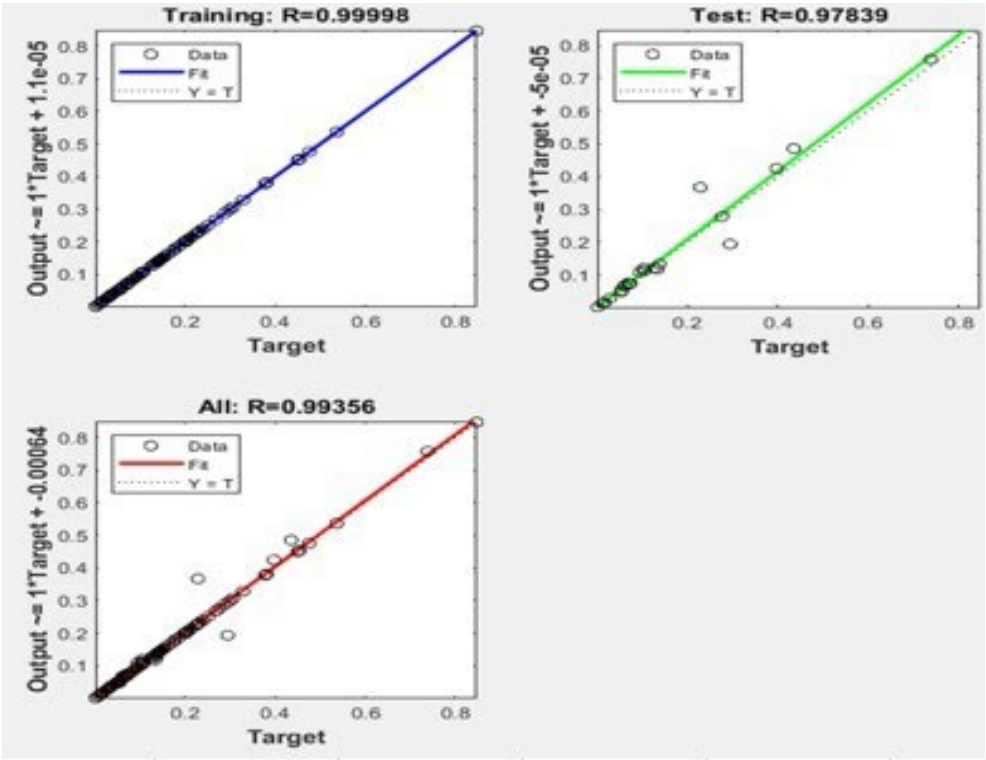


(**a**) (**b**)

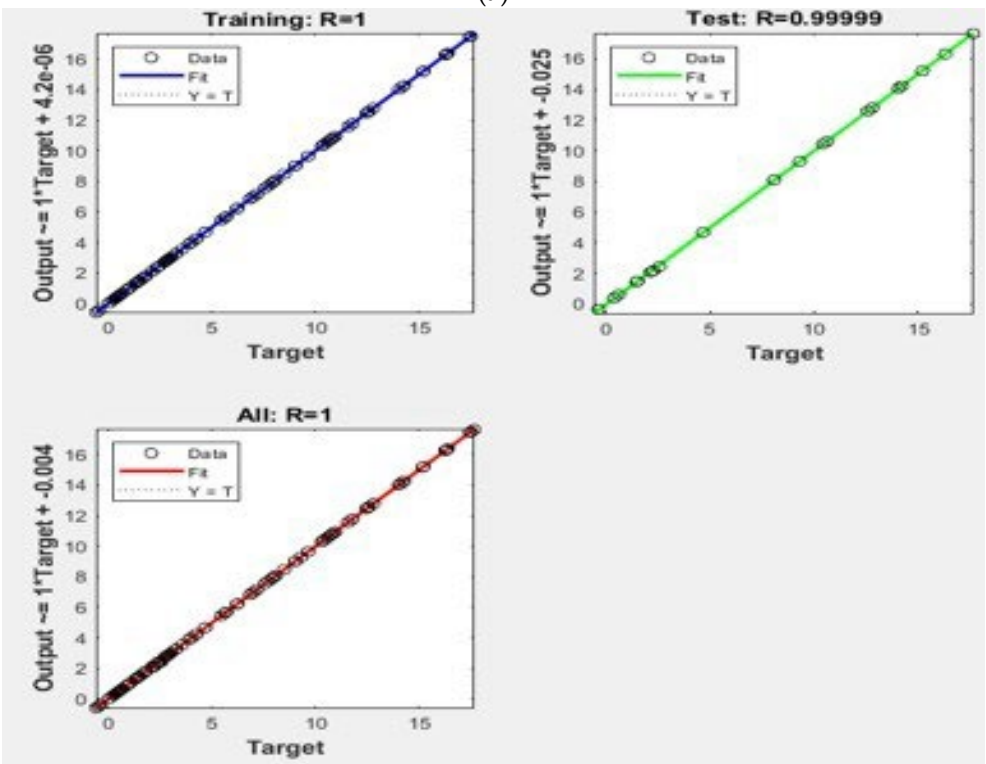
Figure 15. Training performance. (**a**): θ (°); (**b**): PEEQ.

The scaled conjugate gradient algorithm showed lower overall predictive performance, mainly due to its lower validation correlation values, although some error values remained comparable for specific outputs. For PEEQ prediction, the Levenberg-Marquardt algorithm converged rapidly during training, but its validation and test performance were less consistent, suggesting a reduced generalization capability compared with the training response (Figure 15b).

However, Bayesian regularization demonstrated superior generalization with a reduced mean squared error (MSE) on the validation data, as evidenced by the regression plots shown in Figure 16.



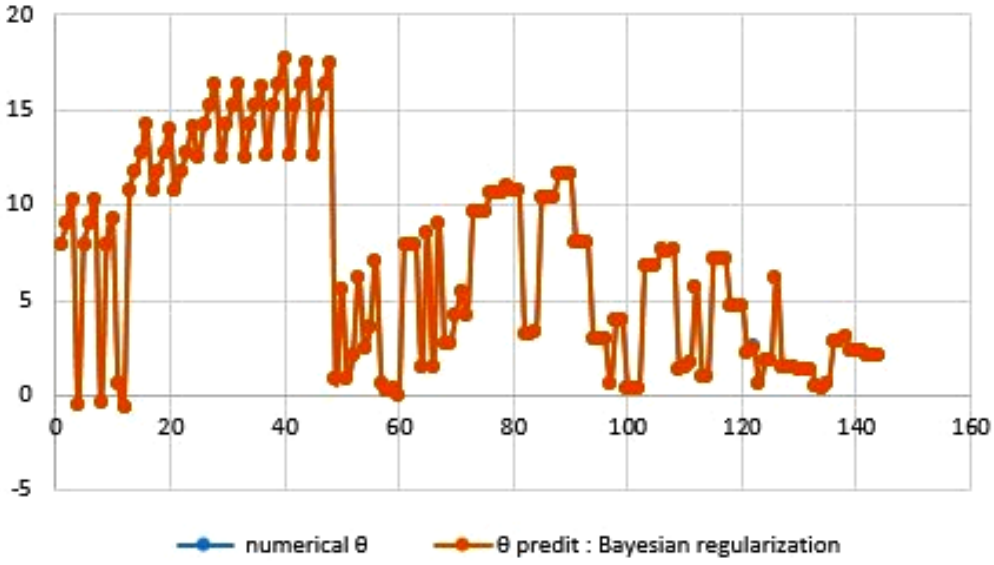
(**a**)



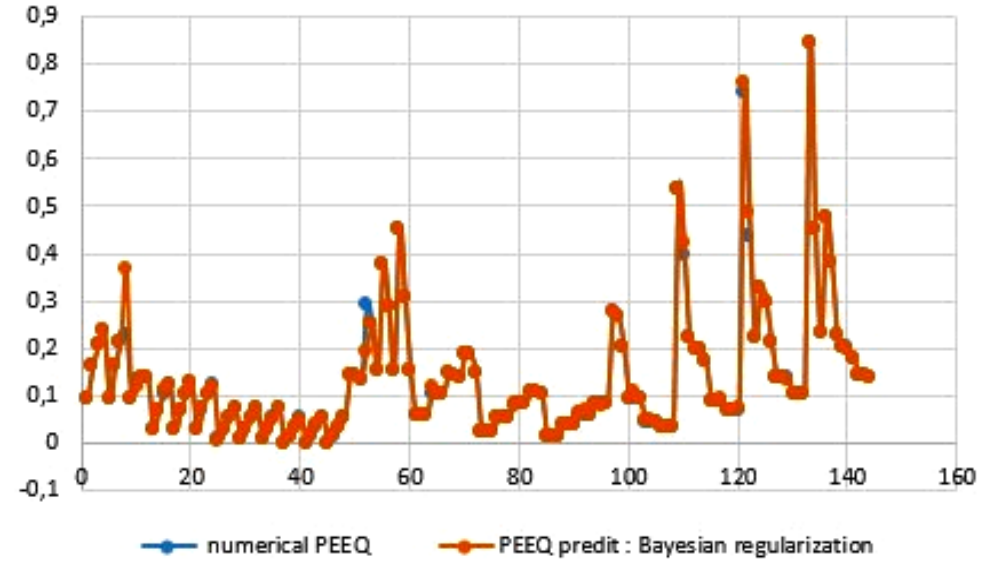
(**b**)

Figure 16. Predictive accuracy. (**a**): θ (°) and (**b**) PEEQ.

Bayesian regularization has been shown to be an effective method of minimizing mean square error (MSE) during training and validation phases, with results comparable to those achieved by the Levenberg-Marquardt algorithm. However, it has been observed to demonstrate enhanced stability and efficacy during the testing phase, as evidenced by regression plots and comparisons of predicted and experimental curves (Figure 17). In contrast, the scaled conjugate gradient algorithm has been found to be less reliable overall.



(**a**)



(**b**)

Figure 17. Comparison between numerical results and Bayesian-regularization predictions for (**a**) spring back and (**b**) PEEQ.

Overall, Bayesian regularization showed the best predictive performance among the tested algorithms for both spring back and PEEQ, as illustrated in Figure 17. Within the present experimental configuration, it provided the most favorable compromise between prediction accuracy, generalization capability, and mean squared error. Although all three algorithms demonstrated promising results, Bayesian regularization appeared to be the most suitable approach for the two considered outputs. Further improvements could still

be achieved by optimizing the network architecture, tuning the training parameters, and enlarging the dataset.

4. Discussion

This study adopted a combined experimental, numerical, and AI-based approach to analyze and optimize the V-bending of Grade 4 titanium plates for orthopedic applications. The results showed that sheet thickness and die shoulder distance are the dominant parameters controlling equivalent plastic strain and spring back. The overall trends obtained from the simulations are consistent with the mechanical characterization and with previous studies on bending and spring back [17,18,25]. More specifically, the strong influence of sheet thickness observed in the present study is consistent with previous investigations showing that an increase in thickness generally reduces springback because of the associated increase in bending stiffness and the modification of the stress distribution through the sheet thickness. The marked effect of die shoulder distance is also mechanically meaningful, since this parameter controls the bending severity and the contact conditions between the sheet and the tools, thereby directly affecting both strain localization and elastic recovery. By contrast, punch radius and punch displacement showed less pronounced effects within the investigated parameter range, which suggests that their contribution is more secondary under the present forming conditions.

The ANN results further support the feasibility of data-driven prediction for V-bending responses, in agreement with previous studies reporting the usefulness of neural-network-based approaches for springback estimation and process optimization [9,10,13]. Among the tested algorithms, Bayesian regularization showed the best overall predictive performance, suggesting that it is a promising approach for predicting springback and PEEQ from the main process parameters, namely sheet thickness, die shoulder distance, punch radius, and punch displacement. In addition to the dominant effects of sheet thickness and die shoulder distance, punch radius and punch displacement also influenced springback and plastic strain, although their contributions were less pronounced, which is consistent with previous studies emphasizing the role of tool geometry and process conditions in bending operations [2,10,13,19]. Nevertheless, the remaining discrepancies between numerical and predicted results indicate that further improvements could be achieved by incorporating anisotropic constitutive behavior and enlarging the dataset used for training.

5. Conclusions

This study demonstrated that a combined experimental, numerical, and ANN-based methodology can be used to analyze the V-bending behavior of Grade 4 titanium plates for orthopedic applications. Among the investigated parameters, sheet thickness and die shoulder distance were found to have the strongest influence on equivalent plastic strain and spring back. The proposed framework therefore provides a useful basis for process optimization in titanium plate forming, since sheet thickness and die shoulder distance were identified as the most influential parameters controlling springback and equivalent plastic strain, whereas punch radius and punch displacement showed less pronounced effects within the investigated range. However, further work is still required to improve the constitutive description of the material and to strengthen the predictive validation of the ANN models before extending the approach to direct crack-risk assessment and implant manufacturing optimization.

Author Contributions: Conceptualization. H.G., S.C. and M.A.T.; Methodology. H.G., S.C. and M.A.T.; Validation. S.C. and M.A.T.; Formal analysis. H.G. and S.C.; Data curation. H.G. and S.C.; Writing—original draft. H.G.; Writing—review & editing. B.L. and M.A.T.; Visualization. B.L., S.C. and M.A.T.; Supervision. M.A.T.; Project administration. B.L. All authors have read and agreed to the published version of the manuscript.

Funding: This work was supported and funded by the Deanship of Scientific Research at Imam Mohammad ibn Saud Islamic University (IMSIU) (grant number IMSIU-DDRSP2503).

Data Availability Statement: The original contributions presented in this study are included in the article. Further inquiries can be directed to the corresponding author.

Conflicts of Interest: The authors declare no conflict of interest.

References

1. Noder, J.; Dykeman, J.; Butcher, C. New methodologies for fracture detection of automotive steels in tight radius bending: Application to the VDA 238–100 V-bend test. *Exp. Mech.* **2021**, *61*, 367–394. [CrossRef]
2. Leu, D.K. A simplified approach for evaluating bendability and spring back in plastic bending of anisotropic sheet metals. *J. Mater. Process. Technol.* **1997**, *66*, 9–17. [CrossRef]
3. Lu, F.; Ma, Q.; Liu, E.; Wei, R.; Bai, J.; Gao, Q.; Qi, J. Advancements in understanding the microstructure and properties of additive manufacturing Ti-6Al-4V alloy: A comprehensive review. *J. Alloys Compd.* **2025**, *1027*, 180543. [CrossRef]
4. Usha Rani, S.; Kesavan, D.; Kamaraj, M. Evaluation of influence of microstructural features of LPBF Ti-6Al-4 V on mechanical properties for an optimal strength and ductility. *J. Alloys Compd.* **2023**, *960*, 170575. [CrossRef]
5. Wahed, M.A.; Gupta, A.K.; Gadi, V.S.R.; Supradeepan, K.S.; Singh, S.K.; Kotkunde, N. Parameter optimization in V-bending process at elevated temperatures to minimize spring back in Ti-6Al-4V alloy. *Adv. Mater. Process. Technol.* **2020**, *6*, 350–364. [CrossRef]
6. Zhao, K.M.; Lee, J.K. Finite element analysis of the three-point bending of sheet metals. *J. Mater. Process. Technol.* **2002**, *122*, 6–11. [CrossRef]
7. Chan, W.M.; Chew, H.I.; Lee, H.P.; Cheok, B.T. Finite element analysis of spring-back of V-bending sheet metal forming processes. *J. Mater. Process. Technol.* **2004**, *148*, 15–24. [CrossRef]
8. Fei, D.; Hodgson, P. Experimental and numerical studies of spring back in air V-bending process for cold rolled TRIP steels. *Nucl. Eng. Des.* **2006**, *236*, 1847–1851. [CrossRef]
9. Inamdar, M.V.; Date, P.P.; Desai, U.B. Studies on the prediction of spring back in air vee bending of metallic sheets using an artificial neural network. *J. Mater. Process. Technol.* **2000**, *108*, 45–54. [CrossRef]
10. Fahle, S.; Prinz, C.; Kuhlenkötter, B. Systematic review on machine learning (ML) methods for manufacturing processes: Identifying artificial intelligence (AI) methods for field application. *Procedia CIRP* **2020**, *93*, 413–418. [CrossRef]
11. Hanoon, A.N.; Al Zand, A.W.; Yaseen, Z.M. Designing new hybrid artificial intelligence model for CFST beam flexural performance prediction. *Eng. Comput.* **2022**, *38*, 3109–3135. [CrossRef]
12. Bandyopadhyay, A.; Mitra, I.; Goodman, S.B.; Kumar, M.; Bose, S. Improving biocompatibility for next generation of metallic implants. *Prog. Mater. Sci.* **2023**, *133*, 101053. [CrossRef] [PubMed]
13. Belay, A.S.; Tsegaw, F.G.; Gebeyehu, S.G. Optimization of Process Parameters Using Taguchi and ANOVA. *J. Eng. Ind. Res.* **2024**, *5*, 152–162. [CrossRef]
14. Marin, E.; Lanzutti, A. Biomedical Applications of Titanium Alloys: A Comprehensive Review. *Materials* **2024**, *17*, 114. [CrossRef] [PubMed]
15. Li, H.; Chen, S.-F.; Zhang, S.-H.; Xu, Y.; Song, H.-W. Deformation Characteristics, Formability and Springback Control of Titanium Alloy Sheet at Room Temperature: A Review. *Materials* **2022**, *15*, 5586. [CrossRef] [PubMed]
16. Wang, S.; Li, W.; Huang, Z.; Li, S.; Zhang, G.; Yu, H. The Action Mechanism of Rolling Texture on the Anisotropic Behavior of a Pure Titanium Plate. *Metals* **2024**, *14*, 849. [CrossRef]
17. Choudhury, I.A.; Ghomi, V. Spring back reduction of aluminum sheet in V-bending dies. *Proc. Inst. Mech. Eng. Part B J. Eng. Manuf.* **2014**, *228*, 917–926. [CrossRef]
18. Thipprakmas, S.; Phanitwong, W. Process parameter design of spring-back and spring-go in V-bending process using the Taguchi technique. *Mater. Des.* **2011**, *32*, 4430–4436. [CrossRef]
19. Ouled Ahmed Ben Ali, R.; Chatti, S. Modeling Spring back of thick sandwich panel using RSM. *Int. J. Adv. Manuf. Technol.* **2019**, *103*, 3375–3387. [CrossRef]
20. Xiaoyan, L.; Lei, L.; Jianguo, L. Mechanical properties and deformation mechanisms of gradient nanostructured metals and alloys. *Nat. Rev. Mater.* **2020**, *5*, 706–723. [CrossRef]

21. Yang, Y.; Huang, W.; Ma, Y.-E.; Wang, S.; Chen, X.; Meng, Y. Mechanical properties and failure modes of additively manufactured Ti6Al4V lattice structures under quasi-static compressive loading. *Int. J. Appl. Mech.* **2022**, *14*, 2250081. [CrossRef]
22. Ahn, K. Plastic bending of sheet metal with tension/compression asymmetry. *Int. J. Solids Struct.* **2020**, *204–205*, 65–80. [CrossRef]
23. *ASTM E8/E8M*; Standard Test Methods for Tension Testing of Metallic Materials. ASTM International: West Conshohocken, PA, USA, 2013; pp. 1–28. [CrossRef]
24. Hu, H.; Wang, X.-Y. Effect of heat treatment on the in-plane anisotropy of as-rolled 7050 aluminum alloy. *Metals* **2016**, *6*, 79. [CrossRef]
25. Tekaslan, Ö.; Gerger, N.; Şeker, U. Determination of spring-back of stainless-steel sheet metal in V-bending dies. *Mater. Des.* **2008**, *29*, 1043–1050. [CrossRef]

Disclaimer/Publisher's Note: The statements, opinions and data contained in all publications are solely those of the individual author(s) and contributor(s) and not of MDPI and/or the editor(s). MDPI and/or the editor(s) disclaim responsibility for any injury to people or property resulting from any ideas, methods, instructions or products referred to in the content.